Spatial Environment Affects *HNF4A* Mutation-Specific Proteome Signatures and Cellular Morphology in hiPSC-Derived β-Like Cells

Manuel Carrasco,[1,2] Chencheng Wang,[3,4] Anne M. Søviknes,[1] Yngvild Bjørlykke,[1,5] Shadab Abadpour,[3,4] Joao A. Paulo,[6] Erling Tjora,[1,5] Pål Njølstad,[1,5] Jonas Ghabayen,[1] Ingrid Nermoen,[7] Valeriya Lyssenko,[1] Simona Chera,[1] Luiza M. Ghila,[1] Marc Vaudel,[1] Hanne Scholz,[3,4] and Helge Ræder[1,5]

Diabetes 2022;71:862–869 | https://doi.org/10.2337/db20-1279

Studies of monogenic diabetes are particularly useful because we can gain insight into the molecular events of pancreatic β-cell failure. Maturity-onset diabetes of the young 1 (MODY1) is a form of monogenic diabetes caused by a mutation in the *HNF4A* gene. Human-induced pluripotent stem cells (hiPSCs) provide an excellent tool for disease modeling by subsequently directing differentiation toward desired pancreatic islet cells, but cellular phenotypes in terminally differentiated cells are notoriously difficult to detect. Re-creating a spatial (three-dimensional [3D]) environment may facilitate phenotype detection. We studied MODY1 by using hiPSC-derived pancreatic β-like patient and isogenic control cell lines in two different 3D contexts. Using size-adjusted cell aggregates and alginate capsules, we show that the 3D context is critical to facilitating the detection of mutation-specific phenotypes. In 3D cell aggregates, we identified irregular cell clusters and lower levels of structural proteins by proteome analysis, whereas in 3D alginate capsules, we identified altered levels of glycolytic proteins in the glucose sensing apparatus by proteome analysis. Our study provides novel knowledge on normal and abnormal function of HNF4A, paving the way for translational studies of new drug targets that can be used in precision diabetes medicine in MODY.

Heterozygous mutations in the *HNF4A* gene are associated with maturity-onset diabetes of the young 1 (MODY1) (1), a monogenic autosomal-dominant type of diabetes. Given the inaccessibility of human pancreatic tissue and insufficient recapitulation of the human phenotype of MODY1 in current in vivo models (2), human-induced pluripotent stem cells (hiPSCs) provide an excellent alternative source to study patient-derived models of MODY1. Previous studies of hiPSC-based models of MODY1 (3–5) have not demonstrated mutation-specific cellular phenotypes in end-stage pancreatic β-like cells. Notably, protocol-optimizing experiments to improve directed pancreatic β-cell differentiation have used three-dimensional (3D) environment strategies (6) where cell aggregation (7,8) and alginate encapsulation (9) have detected better morphological and functional outcomes. In this study, we assessed the properties of mutated and corrected *HNF4A* hiPSC-derived pancreatic β-like cells in two different 3D environments (AggreWell aggregate condition and alginate encapsulation) to demonstrate mutation-specific phenotypes in β-like cells in MODY1.

RESEARCH DESIGN AND METHODS

Cell Source and Reprogramming

We reprogrammed fibroblast cells as previously described (4,10) from a donor from the Norwegian MODY Registry

[1]Department of Clinical Science, University of Bergen, Bergen, Norway
[2]Center for Cancer Biomarkers, Department of Clinical Medicine, University of Bergen, Bergen, Norway
[3]Department of Transplant Medicine and Institute for Surgical Research, Oslo University Hospital, Oslo, Norway
[4]Hybrid Technology Hub–Centre of Excellence, Institute of Basic Medical Sciences, University of Oslo, Oslo, Norway
[5]Department of Pediatrics, Haukeland University Hospital, Bergen, Norway
[6]Department of Cell Biology, Harvard Medical School, Boston, MA
[7]Department of Endocrinology, Akershus University Hospital, Lorenskog, Norway

Corresponding author: Helge Ræder, helge.rader@uib.no

Received 23 December 2020 and accepted 3 January 2022

This article contains supplementary material online at https://doi.org/10.2337/figshare.17836400.

M.C., C.W., A.M.S., and Y.B. contributed equally to this work.

after written informed consent and with experiments approved by the Regional Committee on Medical Ethics of Western Norway (REK 2010/2295). We used isolated human pancreatic islets from three deceased donors without diabetes (REK 2011/782) and the human embryonic stem cell line H1 as control.

Genome Editing

Alt-R CRISPR/Cas9 reagents were provided by Integrated DNA Technologies (Coralville, IA). Briefly, 10^5 iPSCs were mixed with 12.5 μL ribonucleoprotein, 5 μL electroporation enhancer, and 2.5 μL homology-directed repair (HDR) template (stock 3 nmol/L) in 40 μL Nucleofector solution 2 (Lonza); electroporated; and subsequently incubated for 48 h. Dissociated single cells were grown until colonies emerged. Ninety-six colonies were picked and screened. Positive clones from restriction fragment–length polymorphism assay, using BccI enzyme on exon 7–amplified segments, were validated by Sanger sequencing. Seven colonies, including D13, D94, E75, and E87, were found to be corrected by the HDR template.

Evaluation of iPSC Integrity

We characterized iPSCs as previously described (10), including assessment by flow cytometry and immunofluorescence as described below. The chromosome analysis was done at the Cell Guidance Systems Genetics Service, Cytogenetic Laboratory, Babraham Research Campus, Cambridge, U.K. We further evaluated pluripotency potential in mutated and corrected hiPSC lines using an hPSC functional identification kit (SC027B; Bio-Techne Ltd.). Specifically, three uniquely formulated media were used to differentiate hPSCs into the three germ layers endoderm, ectoderm, and mesoderm. The three germ layers were detected by immunocytochemistry using the antibodies for the transcription factors SOX17 (endoderm), Otx2 (ectoderm), and brachyury (mesoderm) (SC027B; Bio-Techne).

Directed Differentiation

The directed differentiation of hiPSCs to β-like cells was performed as previously described (4,11). To reduce variability, we performed the different directed differentiations in parallel in the same multiwell plate for all conditions with the same batch of differentiation cocktail. At the end of stage 5 (S5), 5.0 million cells were embedded in alginate beads, as previously described (12), 1.2 million cells were used to form cell aggregates (8), and ∼5 million cells were kept in adherent culture. The beads, aggregates, and planar cultures were differentiated until stage 7 (S7), as previously described (4,9).

Western Blotting, Flow Cytometry, Immunofluorescence, and Confocal Staining

As described elsewhere, we performed, Western blotting (13), flow cytometry (14), immunofluorescence (4), and confocal imaging (9). For Western blotting, we used the primary antibodies HNF4A (1:1,000; Cell Signaling Technology), PDX1 (1:1,000, R&D Systems), or GAPDH (1:1,000, Santa Cruz Biotechnology); otherwise, we used the following: mouse anti-Oct-3/4 (sc-5279; Santa Cruz Biotechnology), rabbit anti-NANOG (ab21624; Abcam), goat anti-SOX17 (AF1924; R&D Systems), goat anti-PDX1 (AF2419; R&D Systems), mouse anti-HNF4A (PP-H1415-00; R&D Systems), mouse anti-Nkx-6.1 (F55A12-S; Developmental Studies Hybridoma Bank, University of Iowa), and guinea pig anti-insulin (A0564; Dako). The samples were mounted in Prolong Diamond Antifade Mounting Media (P36970; Life Technologies).

Aggregate and Alginate Formation and Processing

We used AggreWell 400 (34411; STEMCELL Technologies) as recommended by the manufacturer. Briefly, 1.2×10^6 cells were seeded per AggreWell in stage 6 (S6) medium, which generated aggregates of ∼1,000 cells. After 48 h incubation, the aggregates were transferred to low-adherence plates and kept on an orbital shaker (100 rpm). We encapsulated cells with alginate and processed the capsules as described elsewhere (9).

RNA Extraction, Processing and Next-Generation RNA Sequencing

RNA was extracted from 2D Matrigel-differentiating cells, aggregates, and encapsulated cells using an RNeasy Micro Kit (QIAGEN) and processed and sequenced (mRNA sequencing for AggreWell samples and 3′ RNA transcriptomics [QIAseq UPX 3′ Transcriptome Kit; QIAGEN] for alginate samples; 2.5 and 10 ng purified RNA for the alginate and 2D samples, respectively) as previously described (9).

Proteomics and Pathway Analysis

The lysed cells and human islets (positive control) were processed and analyzed with mass spectrometry as previously described (4,15), using 25 μg of each sample and three TMT11plexes, with a reference mix of all samples in 2 of the 11 samples in each plex to allow crossplex analysis. Pathway analysis was performed as previously described (4).

Glucose-Stimulated Insulin Secretion and Oxygen Consumption Rate Assays

As previously described, we assessed S7 cells by assays of static glucose-stimulated insulin secretion (GSIS) (4), dynamic GSIS (16), and oxygen consumption rate (OCR) (17) using 60 handpicked S7 cell clusters in dynamic GSIS (perfused with high glucose [20 mmol/L] from 42 to 84 min, whereas other fractions were exposed to low glucose [1.67 mmol/L]) and 40–60 S7 cell clusters per 24 wells during OCR. The final concentrations of 20 mmol/L glucose, 5 μmol/L oligomycin (Cell Signaling Technology), 5 μmol/L carbonyl cyanide 3-chlorophenylhydrazone (Sigma-Aldrich), and 5 μmol/L rotenone (Sigma-Aldrich) were added in order. The OCR values were normalized to

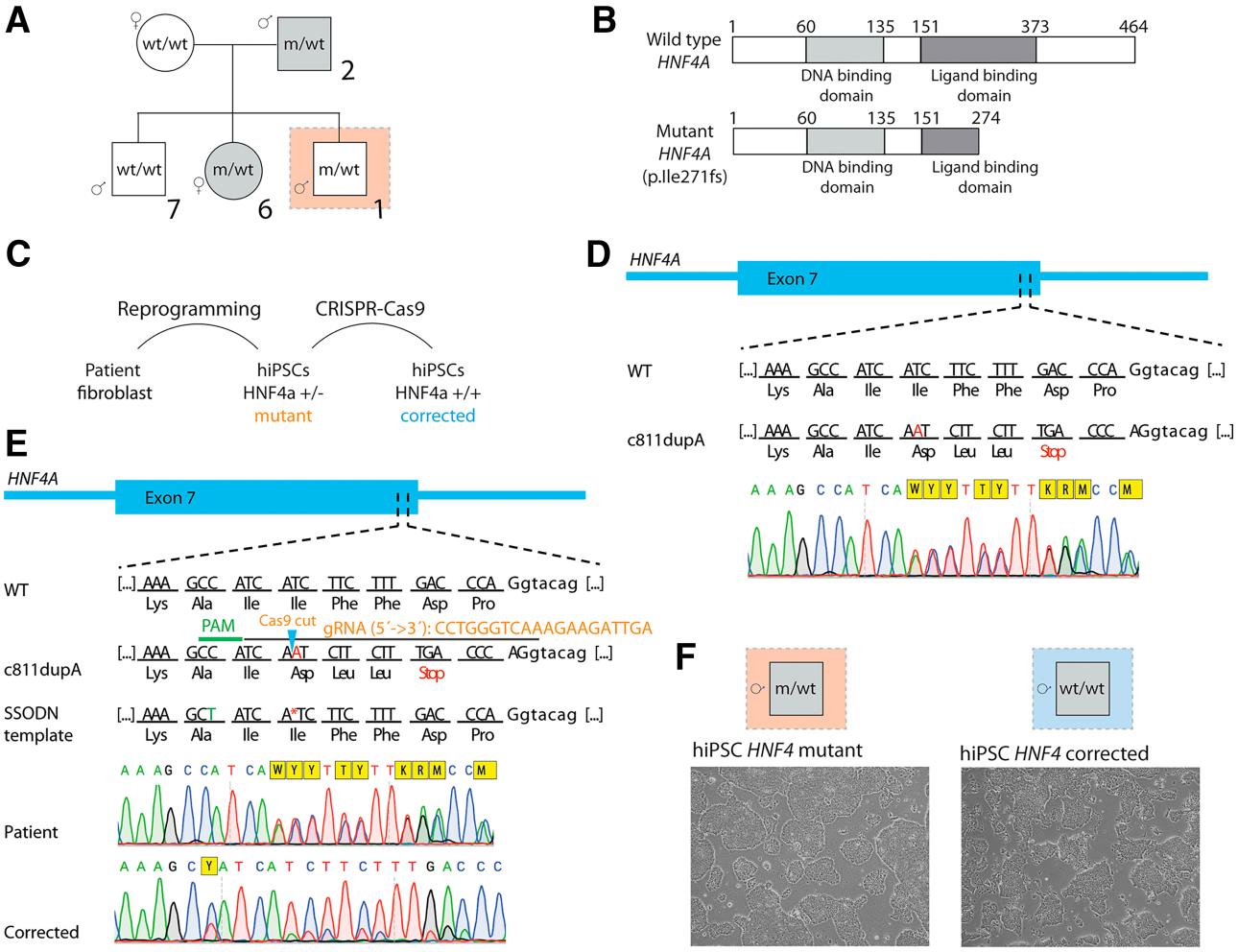

Figure 1—CRISPR/Cas9-mediated correction of an *HNF4A* mutation. *A*: The MODY1 family (N904) with the c.811dupA/p.Ile271fs mutation, showing patient N904-1 (red frame) whose fibroblasts were reprogrammed into hiPSCs. Supplementary Table 1 describes the clinical characteristics of this Norwegian family carrying the *HNF4A* mutation c.811dupA/p.Ile271fs (4). *B*: HNF4A wild-type primary protein structure and the truncated HNF4A primary protein caused by the c.811dupA/p.Ile271fs, resulting in a premature truncation of the protein and consisting of 274 amino acids compared with 464 amino acids in the wild-type normal-length protein. *C*: Schematic overview of study cell line generation. *D*: Diagram of the c.811dupA/p.Ile271fs mutation causing a premature stop codon eight nucleotides downstream and the corresponding chromatogram (by Sanger sequencing) of the mutated clone (*HNF4A*$^{+/c811dupA}$; 6D). *E*: Mutation correction strategy mediated by CRISPR/Cas9-stimulated HDR, showing restoration of the normal genetic sequence after HDR in the corrected clone (*HNF4A*$^{+/corrected}$; E75). See Supplementary Fig. 2 for further details. *F*: Phase-contrast images of representative mutated (*HNF4A*$^{+/c811dupA}$; 6D) and corrected (*HNF4A*$^{+/corrected}$; E75) colonies. m, mutated; SSODN, single-stranded oligodeoxyribonucleotide; wt/WT, wild type.

the average baseline values measured in assay media containing 1.67 mmol/L glucose.

Statistics

Statistical analysis was performed in Excel version 14.7.7 and GraphPad Prism 7.0.0 software. A two-sided *t* test was used, and $P < 0.05$ was considered significant. Supplementary Fig. 11 was built in R 3.6.1 using the packages tidyr version 1.1.3, dplyr version 1.0.0, scico version 1.2.0, and ggplot2 version 3.3.5.

Data and Resource Availability

The RNA-sequenced data sets have been deposited in the National Center for Biotechnology Information Gene Expression Omnibus (accession no. GSE188827). The proteome data sets have been deposited in ProteomeXchange through the Proteomics Identification Database (accession no. PXD025054).

RESULTS

Generation of Mutated and Isogenic Control Cell Lines Using MODY1 iPSCs With an *HNF4A* Mutation

We generated several mutated (*HNF4A*$^{+/c811dupA}$) hiPSC lines (the hiPSC lines 6A, 6D, and 6F in Supplementary Fig. 1) by reprogramming fibroblasts from a patient with MODY1 (N904-1 in Fig. 1*A* and Supplementary Table 1) with a c.811dupA/p.Ile271fs mutation (Fig. 1*B*). Using these lines, we created corrected (*HNF4A*$^{+/corrected}$)

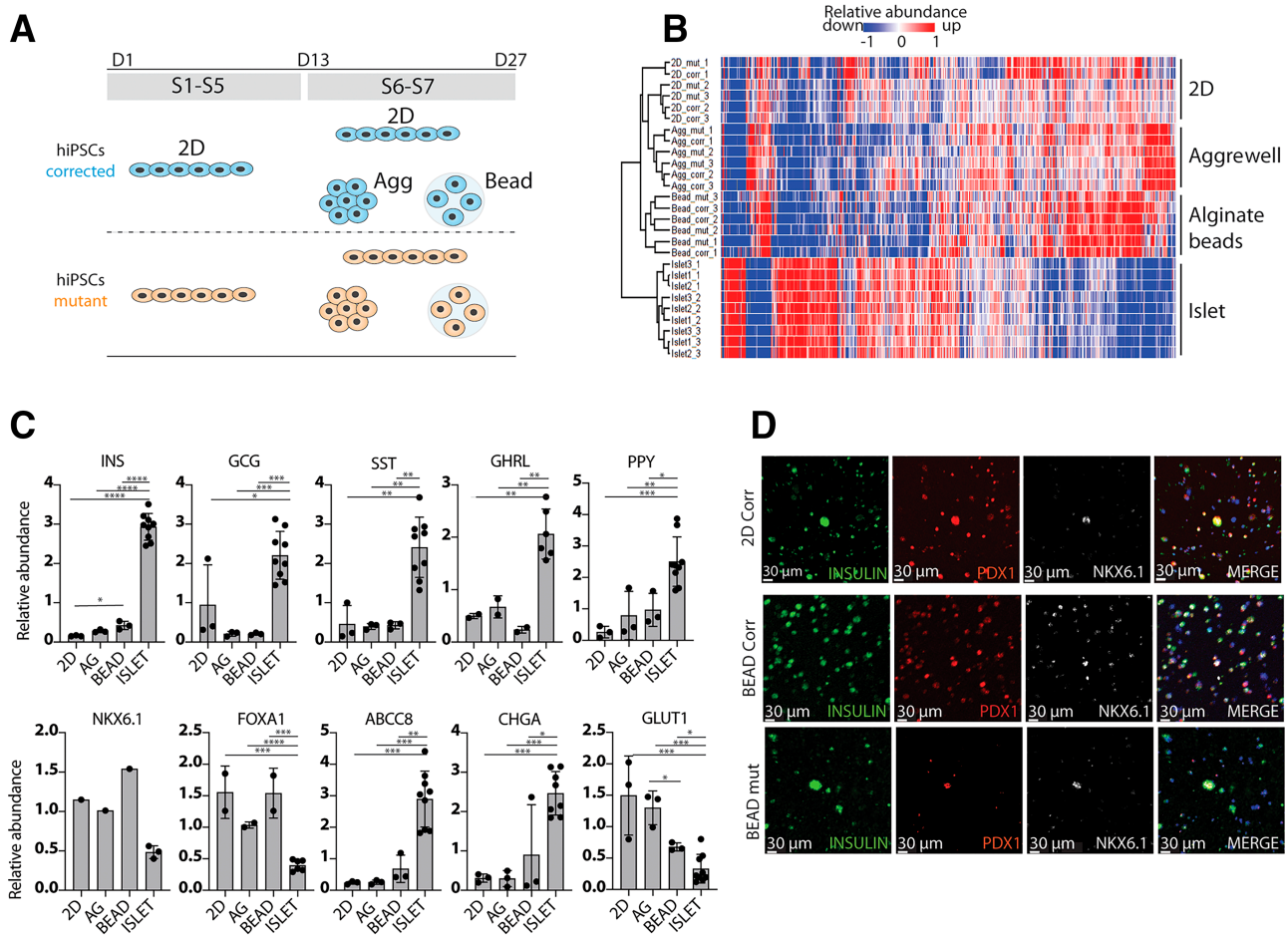

Figure 2—The 3D environments have a major impact on the cellular proteome. *A*: Schematic overview of the experimental design. We modified the last stages (S6–S7) in the protocol to allow the formation of two 3D environments (aggregate formation generating cell aggregates and alginate encapsulation generating "beads") in addition to the 2D monolayer environment. At S6, the cells were either encapsulated in alginate (3D), organized in size-adjusted cell aggregates by the use of AggreWell (3D), or maintained in the traditional 2D monolayer configuration (negative control). *B*: Hierarchical clustering analysis of all the lines in different 2D and 3D environments and of human islet controls in the global proteomic analysis (Euclidian distance) using an 11plex-based global quantitative proteomics approach. We were able to quantify 8,173 proteins in total and focused our subsequent analyses on a threshold defined as proteins quantified in at least 20 of 27 samples (6,127 proteins). Hierarchical clustering analyses revealed that cell lines differentiated in the same 3D environment clustered together, yielding unique proteomic signatures, with the proteomic signature of alginate-encapsulated cell lines (alginate beads) being most similar to that of human islets as demonstrated previously (9). *C*: The relative abundance levels (based on proteomics measurements of single-protein levels) of hormones and key β-cell markers in alginate-encapsulated cells, aggregates, and 2D-cultivated cells compared with human islets. *D*: The expression of the pancreatic β-cell markers INS, PDX1, and NKX6.1 in alginate-encapsulated cells and in 2D-cultivated cells analyzed by immunocytochemistry. AG/Agg, aggregates; Aggre, AggreWell; corr, corrected; mut, mutant.

mutation-free isogenic hiPSC lines (the E75, D13, D94, E87 hiPSC lines in Supplementary Fig. 1) by CRISPR/Cas9 HDR gene editing (Fig. 1*C*–*E* and Supplementary Figs. 2–3). We subsequently assessed the integrity of the mutated and corrected hiPSC lines (10) (Fig. 1*F* and Supplementary Figs. 1 and 4–7).

The 3D Environment Influences the Composition of the Cellular Proteome

The mutated and corrected hiPSCs were subjected to directed differentiation (Supplementary Fig. 8) toward pancreatic β-like cells, as done previously (4), but by adding two different 3D environments (aggregate formation in AggreWell and alginate encapsulation) to the standard 2D format (Fig. 2*A*). Using global proteomics analysis of end-stage pancreatic β-like cells (S7), we found that the cell lines cultured in AggreWell or in alginate capsules yielded distinctively different proteomics signatures (disregarding mutational status) that were also distinctively different from the lines cultured in 2D and from islet controls (Fig. 2*B*). The 2D and 3D environments did not differentially impact the single-protein levels (measured by proteomics) of key β-cell markers (Fig. 2*C* and Supplementary Fig. 9*A*), which were also expressed at a similar level by immunocytochemistry (Fig. 2*D*). Although proteomics analysis of S7 cells did not detect the HNF4A protein, we confirmed

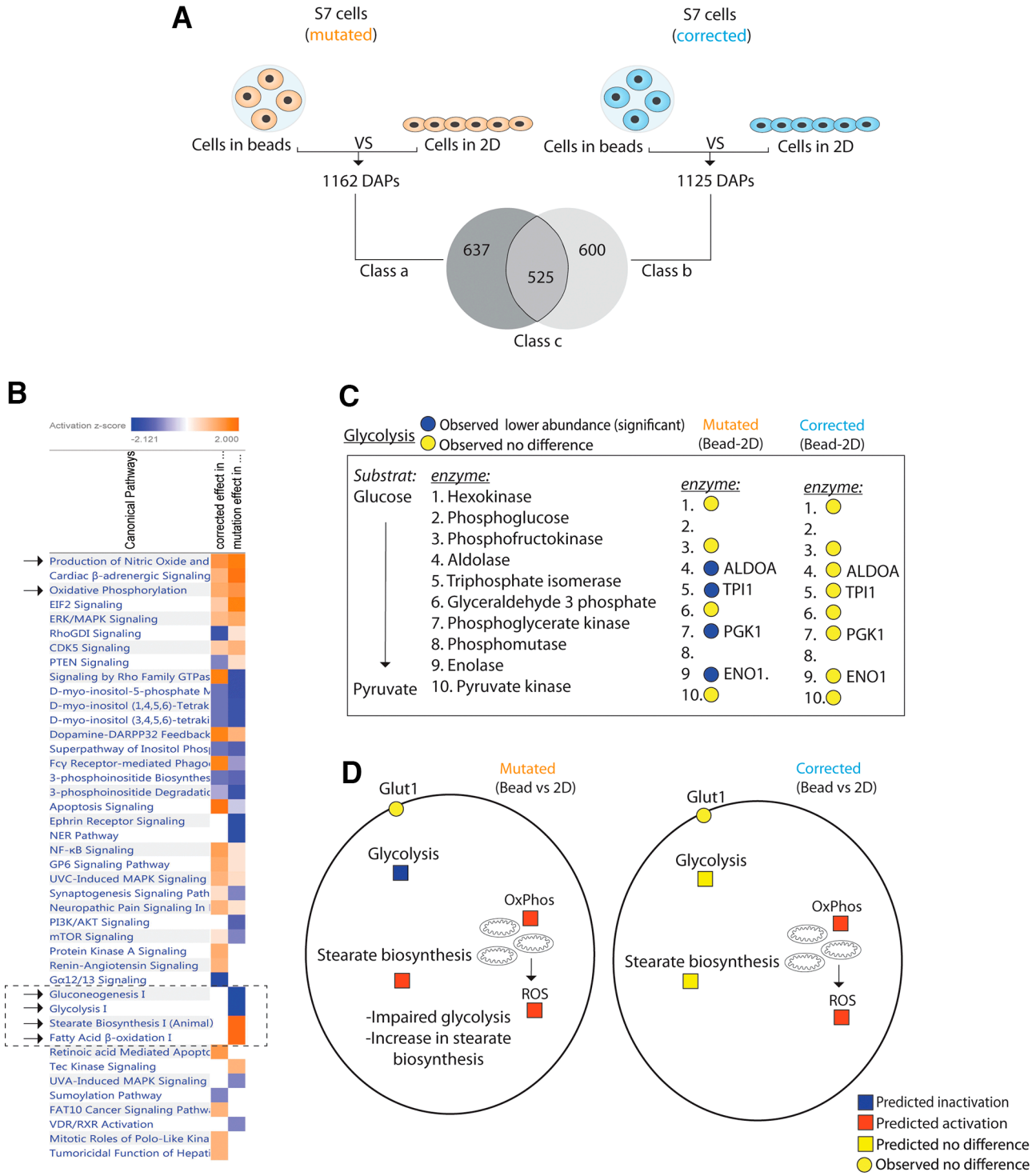

Figure 3—Mutation-specific metabolic switch in the 3D alginate environment. *A*: Schematic overview of the study design where the proteome of cells in 3D alginate beads were compared with the proteome of cells in the 2D format for both the mutated cells (*HNF4A*$^{+/c811dupA}$; 6D) and the corrected (*HNF4A*$^{+/corrected}$; E75) S7 cells, resulting in 1,168 and 1,130 differentially abundant proteins (DAPs) (fold change >1.5; $P < 0.05$), respectively. The DAPs were compared to distinguish the common DAPs caused by the alginate (bead) effect (class c, 525 proteins), DAPs caused by the mutation effect (class a, 637 proteins), and DAPs caused by the corrected effect (class b, 600 proteins). *B*: Top canonical pathways (*z* score >1) identified by analysis of class a DAPs and class b DAPs (*z* score filter = 1). Full canonical pathway names can be found in Supplementary Material. *C*: Sequential events in glycolysis and the observed abundance level of quantified proteins involved in glycolysis in 3D alginate beads compared with 2D (yellow, no difference; blue, significantly lower abundance) demonstrated lower levels of fructose-biphosphate aldolase A (ALDO), α-enolase (ENO1), triphosphate isomerase (TPI1), and phosphoglycerate kinase 1 (PGK1). Although these four proteins are not known to be directly activated by HNF4A, they are all potential targets, as they contain HNF4A binding motifs (25). When we investigated the other parts of the glucose sensing apparatus of pancreatic β-cells in the context of the alginate-encapsulated 3D environment, we did not observe mutation-specific effects either in the levels of proteins involved in glucose influx (GLUT1) or in oxidative phosphorylation (OxPhos) (data not shown). *D*: Schematic illustration summarizing the findings related to a metabolic switch. Observed data are represented by circles, and Ingenuity Pathway Analysis–predicted data are represented by squares. ROS, reactive oxygen species; VS, versus.

HNF4A expression at intermediary stages by other methods (Supplementary Figs. 8 and 10).

The 3D Alginate Encapsulation Environment Potentially Triggers a Mutation-Specific Metabolic Switch

Given that the alginate 3D environment had indeed produced a unique proteomics signature of S7 cells, we next assessed whether the mutational status affected the alginate-encapsulated S7 proteome (Fig. 3*A*). Focusing first on the mutated alginate-encapsulated S7 cells (class a in Fig. 3*A*), we identified glycolysis and gluconeogenesis (predicted as inhibited) as the top canonical pathway, consistent with the known role of HNF4A to regulate metabolic glucose sensing in pancreatic β-cells (18), followed by fatty acid β-oxidation and stearate biosynthesis (predicted as activated) (Fig. 3*B* and Supplementary Fig. 9*B*). In contrast, when extending the pathway analyses to the proteome of corrected cells (class b in Fig. 3*A*), we were not able to predict significant differences in glycolytic and glyconeogenetic pathways or in stearate biosynthesis and fatty acid β-oxidation pathways (Fig. 3*B*), supporting the notion that gene correction rescued the phenotype. Analogously, from the analysis of the proteome data set at the single-protein level (Fig. 3*C* and *D* and Supplementary Fig. 9*C* and *D*), four proteins among 10 enzymes in the glycolytic pathway displayed lower levels in the alginate-encapsulated 3D environment compared with 2D for mutated lines but not in corrected lines, although these were not reproduced in the transcriptome (Supplementary Fig. 11).

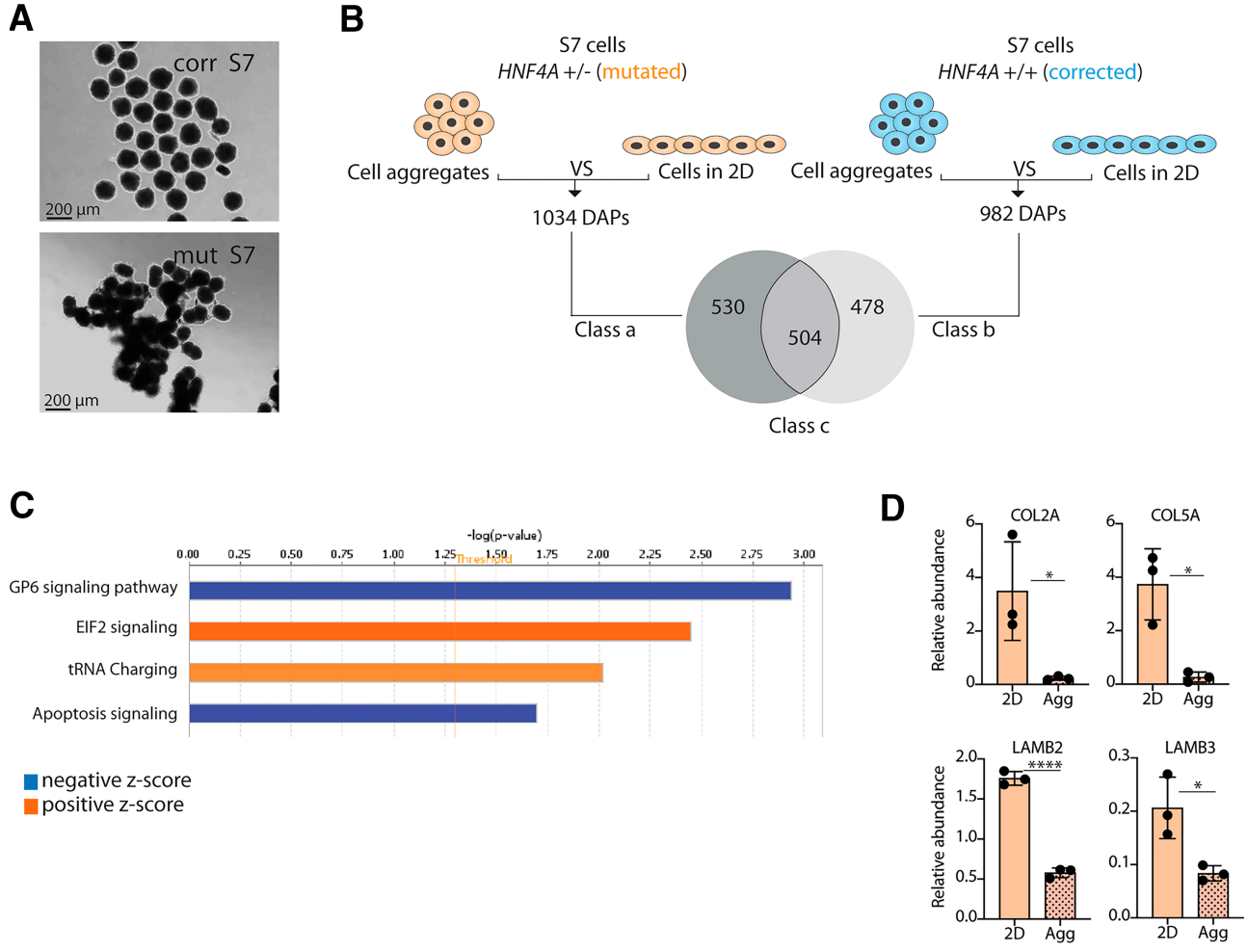

Figure 4—Mutation-specific impaired 3D cell aggregation. *A*: Phase-contrast representative images of mutated (*HNF4A*$^{+/c811dupA}$; 6D) and corrected (*HNF4A*$^{+/corrected}$; E75) S7 cell aggregates. *B*: Schematic overview of the study design where the proteomes of 3D cell aggregates were compared with the 2D proteomes for both the mutated cells and the corrected cells, resulting in 1,034 and 982 differentially abundant proteins (DAPs), respectively (fold change >1.5; $P < 0.05$). The DAPs were compared to distinguish the common DAPs caused by the 3D aggregation effect (class c, 504 proteins), DAPs caused by the mutation effect (class a, 530 proteins), and the DAPs caused by the corrected effect (class b, 478 proteins). *C*: Top canonical pathways (*z* score >1) identified by analysis of class a DAPs. *D*: Selected proteins involved in the GP6 signaling pathway, including collagen 2A (COL2A), collagen 5A (COL5A), and other ECM proteins, including laminin B2 (LAMB2) and LAMB3, were lower in the 3D cell aggregates of mutated cells (*HNF4A*$^{+/c811dupA}$; 6D) compared with mutated cells cultivated in 2D. *$P < 0.05$, ****$P < 0.0001$ by Student *t* test. Agg, aggregate; corr, corrected; mut, mutant; tRNA, transfer RNA; VS, versus.

The 3D Aggregation Cell Environment Precipitates a Mutation-Specific Cellular, Proteome-Specific, and Functional Phenotype

Since we found that also the aggregated 3D environment had produced a unique proteomics signature of S7 cells, we next assessed the mutated AggreWell-cultivated S7 lines. Strikingly, we observed that the mutated lines formed irregular spheroids that clustered together (Fig. 4*A* and Supplementary Fig. 12). In contrast, the corrected lines formed regular round shapes, which did not cluster (Fig. 4*A* and Supplementary Fig. 12). Next, we assessed whether the mutational status affected the alginate-encapsulated S7 proteome and transcriptome (Fig. 4*B* and Supplementary Fig. 11), first focusing on mutated AggreWell-encapsulated S7 cells (class a in Fig. 4*B*). We identified GP6 signaling and apoptosis (predicted inhibition) and EIF2 signaling and transfer RNA (predicted activation) as top canonical pathways (Fig. 4*C*). Since the GP6 signaling pathway plays a role in collagen-induced activation and aggregation (19), we assessed the proteome at the single-protein level and found that indeed, reduced levels of collagen and extracellular matrix (ECM)–related proteins (Fig. 4*D*), validated at the mRNA level (Supplementary Fig. 11). Finally, we assessed and identified mutation-specific functional readouts uniquely present in the aggregated 3D context (Supplementary Fig. 13).

DISCUSSION

In this study, we were able to identify for the first time a mutation-specific phenotype in MODY1 β-like cells facilitated by growing the cells in two different 3D environments and comparing the cellular and proteomic readouts to the 2D background. We were also able to suggest two specific molecular mechanisms whereby the two different 3D culture effects could be mediated. Each of these specific molecular mechanisms showed a dependency on the type of 3D context chosen. The cellular confinement in the alginate context helped to identify a metabolic phenotype with lower levels of glycolytic proteins, potentially affecting glucose sensing. The structural scaffolding in the AggreWell 3D context helped to identify a structural collagen-associated phenotype with irregular clusters, a unique proteome with lower levels of structural ECM proteins (laminins, collagens) as well as a functional readout.

The two chosen 3D environments challenge the differentiating pancreatic β-like cells in unique ways, including the levels of oxygen delivery, nutrient supply, and cell-to-cell contact. The 3D cell aggregation/AggreWell context is preferred by several investigators in generating pancreatic β-like cells (7,8,20) because it mimics the in vivo pancreatic islets in size, level of cell-to-cell contact, and the self-organized compact spheroid arrangement (21). In the 3D alginate encapsulation context, the cells are immobilized and lack cell-to-cell contact; however, the alginate gel-pore network still allows transport of oxygen and diffusion of nutrients and waste products (22). Furthermore, alginate encapsulation is suitable for future therapeutic transplantation (23) and can also protect the cells in bioreactor culture systems (24).

In conclusion, our findings warrants a careful consideration and selection of an appropriate 3D context when studying stem cell models. Our study also provides a patient-specific diabetes model that can be further explored for potential new drug targets that can be used in precision diabetes medicine.

Acknowledgments. The authors thank the Islet Distribution Program at the University of Oslo for providing human islets samples. They also thank Dr. Steven P. Gygi and the Taplin Mass Spectrometry facility at Harvard Medical School for use of mass spectrometers, A.H. Knudsen for technical help, and Lars A. Akslen at the Center for Cancer Biomarkers, Department of Clinical Medicine, University of Bergen, for strategic support. The confocal imaging was performed at the Molecular Imaging Center, Department of Biomedicine, University of Bergen.

Funding. This work was funded by Bergen Forskningsstiftelse (grant BFS2014REK02 to H.R.), Diabetesforbundet (to H.R.), Johan Selmer Kvanes legat (to H.R.), Novo Nordisk Foundation - Komite for Endokrinologi og Metabolisme - Norden (ENDO) (grant NNF17OC0027258 to H.R.), Novo Nordisk Foundation (grant NNF15OC0015054 to S.C.), the Research Council of Norway through its Centres of Excellence funding scheme (project #262613 and project #301178 to M.V.) and Norwegian Research Foundation UiO:LifeScience Convergence Environments II (grant 247577 to H.S.), Western Norway Regional Health Authority (grant 911985 to H.R.), and National Institutes of Health/National Institute of General Medical Sciences (grant R01 GM132129 to J.A.P.).

Duality of Interest. No potential conflicts of interest relevant to this article were reported.

Author Contributions. M.C. performed immunofluorescence imaging and analyses. M.C., C.W., A.M.S., Y.B., S.C., L.M.G., H.S., and H.R. interpreted the observations. M.C., C.W., Y.B., and J.G. performed the differentiation, sample preparation for proteomic and RNA sequencing analyses, and immunofluorescence staining, and analyzed data. M.C., A.M.S., Y.B., V.L., H.S, and H.R. conceived the experiments. C.W. performed the FACS analyses. A.M.S. performed the CRISPR/Cas9 editing and iPSC integrity studies. Y.B. and S.C. analyzed the proteomics data. Y.B., H.S., and H.R. wrote the manuscript. S.A. performed the immunoblotting. S.A. and H.S. generated human islet preparations. J.A.P. performed the tandem mass tag–labeling experiment and mass spectrometry analysis. E.T. provided the skin biopsy samples. E.T., P.N., I.N., and H.R. provided clinical data. M.V. performed the RNA sequencing bioinformatics analyses. All the authors reviewed, commented on, and edited the manuscript. H.R. is the guarantor of this work and, as such, had full access to all the data in the study and takes responsibility for the integrity of the data and the accuracy of the data analysis.

References

1. Yamagata K, Oda N, Kaisaki PJ, et al. Mutations in the hepatocyte nuclear factor-1alpha gene in maturity-onset diabetes of the young (MODY3). Nature 1996;384:455–458

2. Gupta RK, Vatamaniuk MZ, Lee CS, et al. The MODY1 gene HNF-4alpha regulates selected genes involved in insulin secretion. J Clin Invest 2005;115:1006–1015

3. Ng NHJ, Jasmen JB, Lim CS, et al. HNF4A haploinsufficiency in MODY1 abrogates liver and pancreas differentiation from patient-derived induced pluripotent stem cells. iScience 2019;16:192–205

4. Vethe H, Bjørlykke Y, Ghila LM, et al. Probing the missing mature β-cell proteomic landscape in differentiating patient iPSC-derived cells. Sci Rep 2017;7:4780

5. Braverman-Gross C, Nudel N, Ronen D, Beer NL, McCarthy MI, Benvenisty N. Derivation and molecular characterization of pancreatic differentiated MODY1-iPSCs. Stem Cell Res (Amst) 2018;31:16–26
6. Loo LSW, Lau HH, Jasmen JB, Lim CS, Teo AKK. An arduous journey from human pluripotent stem cells to functional pancreatic β cells. Diabetes Obes Metab 2018;20:3–13
7. Balboa D, Saarimäki-Vire J, Borshagovski D, et al. Insulin mutations impair beta-cell development in a patient-derived iPSC model of neonatal diabetes. eLife 2018;7: e38519
8. Nair GG, Liu JS, Russ HA, et al. Recapitulating endocrine cell clustering in culture promotes maturation of human stem-cell-derived β cells. Nat Cell Biol 2019;21:263–274
9. Legøy TA, Vethe H, Abadpour S, et al. Encapsulation boosts islet-cell signature in differentiating human induced pluripotent stem cells via integrin signalling. Sci Rep 2020;10:414
10. Bjørlykke Y, Søviknes AM, Hoareau L, et al. Reprogrammed cells display distinct proteomic signatures associated with colony morphology variability. Stem Cells Int 2019;2019:8036035
11. Ghila L, Bjørlykke Y, Legøy TA, et al. Bioinformatic analyses of miRNA-mRNA signature during hiPSC differentiation towards insulin-producing cells upon HNF4α mutation. Biomedicines 2020;8:179
12. Ghila L, Legøy TA, Chera S. A method for encapsulation and transplantation into diabetic mice of human induced pluripotent stem cells (hiPSC)-derived pancreatic progenitors. Methods Mol Biol. 31 March 2021 [Epub ahead of print]. DOI: 10.1007/7651_2021_356
13. Ræder H, McAllister FE, Tjora E, et al. Carboxyl-ester lipase maturity-onset diabetes of the young is associated with development of pancreatic cysts and upregulated MAPK signaling in secretin-stimulated duodenal fluid. Diabetes 2014;63:259–269
14. Legøy TA, Mathisen AF, Salim Z, et al. In vivo environment swiftly restricts human pancreatic progenitors toward mono-hormonal identity via a HNF1A/HNF4A mechanism. Front Cell Dev Biol 2020;8:109
15. Vethe H, Ghila L, Berle M, et al. The effect of Wnt pathway modulators on human iPSC-derived pancreatic beta cell maturation. Front Endocrinol (Lausanne) 2019;10:293
16. Eich T, Ståhle M, Gustafsson B, et al. Calcium: a crucial potentiator for efficient enzyme digestion of the human pancreas. Cell Transplant 2018;27:1031–1038
17. Zhang E, Mohammed Al-Amily I, Mohammed S, et al. Preserving insulin secretion in diabetes by inhibiting VDAC1 overexpression and surface translocation in β cells. Cell Metab 2019;29:64–77.e6
18. Gonzalez FJ. Regulation of hepatocyte nuclear factor 4 alpha-mediated transcription. Drug Metab Pharmacokinet 2008;23:2–7
19. Andrews RK, Arthur JF, Gardiner EE. Targeting GPVI as a novel antithrombotic strategy. J Blood Med 2014;5:59–68
20. Pagliuca FW, Millman JR, Gürtler M, et al. Generation of functional human pancreatic β cells in vitro. Cell 2014;159:428–439
21. Steiner DJ, Kim A, Miller K, Hara M. Pancreatic islet plasticity: interspecies comparison of islet architecture and composition. Islets 2010;2:135–145
22. Andersen T, Auk-Emblem P, Dornish M. 3D cell culture in alginate hydrogels. Microarrays (Basel) 2015;4:133–161
23. Langhans SA. Three-dimensional in vitro cell culture models in drug discovery and drug repositioning. Front Pharmacol 2018;9:6
24. Miranda JP, Rodrigues A, Tostões RM, et al. Extending hepatocyte functionality for drug-testing applications using high-viscosity alginate-encapsulated three-dimensional cultures in bioreactors. Tissue Eng Part C Methods 2010;16:1223–1232
25. Bolotin E, Liao H, Ta TC, et al. Integrated approach for the identification of human hepatocyte nuclear factor 4alpha target genes using protein binding microarrays. Hepatology 2010;51:642–653